Journal of Materials Chemistry C



COMMUNICATION

View Article Online



Anisothermal densification kinetics of the cold sintering process below 150 °C† Cite this: J. Mater. Chem. C, 2020,

Sun Hwi Bang, 10 * Arnaud Ndayishimiye and Clive A. Randall

8 5668

Received 21st January 2020, Accepted 28th March 2020

DOI: 10.1039/d0tc00395f

rsc.li/materials-c

Cold sintering is an emerging non-equilibrium process methodology that densifies ceramic powders at significantly reduced temperatures. This study proposes a fundamental framework to investigate its densification kinetics. By controlling four densification process variables including the transient chemistry, sintering temperature, uniaxial pressure and dwell time, the anisothermal sintering kinetics of highly densified ZnO is identified and phenomenologically modeled for its relative activation energetics.

Sintering is an important scientific and also industrial processing technique, under which thermal energy and often external pressure are used to transform powder into a solid with enhanced mechanical strength. The fundamental driving force for sintering is the reduction of the excess free energy of the powder surface by increasing the solid/solid interface and also coarsening the grain size.² As ceramic sintering generally requires high temperatures above 1000 °C, decreasing the processing temperature is a technological and environmental challenge. However, one of the immediate advantages of enabling a low temperature process is to explore new ceramic composite designs and properties for various functional material applications.³⁻⁵

Among low-temperature and external pressure ceramic densification methods including spark plasma sintering⁶ and hydrothermal sintering,⁷ the cold sintering process features material densification in an open system8 at significantly reduced processing temperatures, which is enabled by the presence of a transient phase.9 Several technological advantages of cold sintering include (1) preservation of the nanocrystalline size, 10 (2) co-processing of ceramic composites, 11 (3) densification of thermodynamically metastable materials, 12

(4) fabrication of multilayer electroceramics¹³ and (5) significant

Materials Research Institute and Department of Materials Science and Engineering, Pennsylvania State University, University Park, PA, 16802, USA. E-mail: sbang@psu.edu

† Electronic supplementary information (ESI) available. See DOI: 10.1039/

energy reduction.¹⁴ Although its uniaxial pressure requirement has been occasionally regarded as a methodological limitation, the recent size scale-up cold sintering process demonstrated its promising potential in industrial implementation, which can operate below 50 MPa.15

Despite its scientific and technological importance, the fundamental understanding of the cold sintering kinetics and densification mechanisms is still in the very early stages of investigation. Analogous to conventional sintering kinetics studies, ZnO is often employed as a model material system for cold sintering. Its initial sintering potential was first reported in 2015, ¹⁶ and, recently, a combined computational and experimental investigation showed that surface hydroxylation accelerates the dissolved Zn cation adsorption and enhances the diffusion during cold sintering.17 Using grain size based sintering kinetics analysis, the apparent activation energy of ZnO grain growth was only 20% of the value observed in solid state sintering.¹⁸ Moreover, the Kelvin probe force microscopy method showed that the transient liquid accounts for generating highly defective grain boundaries, leading to a reduction of the activation energy of the atomic diffusion.19

The core objectives of understanding sintering kinetics are to predict the densification behavior under different processing conditions and to obtain a uniform microstructure at high density with controlled grain size. In solid state sintering, the constant heating rate of anisothermal sintering is known to influence the densification and grain growth behavior, where a faster heating rate leads to higher densification and finer microstructure at the same temperature due to an increased volumetric strain rate.²⁰ Furthermore, a non-linear sintering temperature has processing advantages for finely regulating the path of morphological change.21 Hence, the proposed study is intended to identify the anisothermal densification kinetics of ZnO cold sintering and to quantify the relevant activation energy. Advancing sintering kinetics knowledge is a necessary condition to develop a complete analytical model, which will certainly accelerate cold sintering composite materials research and application deployment.

Experimental methods

Instrumentation

For any cold sintering process, the transient chemistry $(\mu(t))$, sintering temperature (T), uniaxial pressure (P) and dwell time (t) can be classified as densification process variables (Fig. S1, ESI†). In order to precisely measure the pellet linear shrinkage²² and temperature in each time period, we herein present a new engineering design for collecting the real-time temperature of the pellet during cold sintering (Fig. S2, ESI†). Instrumentation, cold sintering process (Fig. S3, ESI†) and material characterization details are documented in the ESI.†

Mathematical derivation

Among a few reported mathematical models of anisothermal sintering kinetics, 23-26 the Woolfrey-Bannister 27 approach was employed in this study to empirically analyze the activation energy of cold sintering, which has been widely accepted to analyze sintering behaviors of ZnO.²⁸⁻³¹ The general kinetics equation for investigating the initial stage of sintering under a constant heating rate is the following:

$$\frac{\mathrm{d}(\Delta L/L_0)}{\mathrm{d}t} = K_0 \, \exp\left(-\frac{Q}{RT}\right) \left(\frac{L_0}{L}\right)^{-n} \tag{1}$$

where $\Delta L/L_0$ is the linear shrinkage, t is the total time, K_0 is either constant or proportional to 1/T depending on the mass transport mechanism, Q is the apparent activation energy, R is the ideal gas constant, T is the absolute temperature, and n is usually associated with a constant determined from a relatable sintering mechanism. By assuming that the isothermal and anisothermal shrinkage rates are equal and $Q \gg RT$, eqn (1) is approximated by:32

$$\left(\frac{\Delta L}{L_0}\right)^{(n+1)} = \left(\frac{K_0 R T^2 (n+1)}{\alpha Q}\right) \exp\left(-\frac{Q}{R T}\right) \tag{2}$$

where α is a constant heating rate defined as $\alpha = \frac{dT}{dt}$. After further mathematical simplifications, eqn (1) is often used in the following form:27

$$T^{2} \frac{\mathrm{d}(\Delta L/L_{0})}{\mathrm{d}t} = \left(\frac{\alpha Q}{(n+1)R}\right) \left(\frac{\Delta L}{L_{0}}\right) \tag{3}$$

Assuming that Q, n and α are invariant during the anisothermal sintering, taking the natural logarithm of eqn (2) leads to the determination of n:

$$\ln\left(\frac{\Delta L}{L_0}\right) = -\frac{1}{(n+1)}\ln\alpha$$

$$+\frac{1}{(n+1)}\left[\ln\left(K_0RT^2(n+1)\right) - \ln Q - \frac{Q}{RT}\right]$$
(4)

One of the significant advantages of the proposed anisothermal kinetics approach is the direct empirical constitutive relation among linear shrinkage, temperature and time without assuming the values of exponents based on a single diffusion mechanism. However, a crucial assumption for the proposed method is that linear shrinkage is a consequence of material densification, not liquid evaporation, which is verified to be a negligible volume fraction during the cold sintering process.

Results

Anisothermal sintering of ZnO

The relative density evolution³³ and specific surface area reduction²⁸ during anisothermal ZnO cold sintering resemble the basic shape form of the higher temperature solid state sintering process (Fig. 1a). By assuming no powder extrusion and no radial pellet shrinkage taking place during cold sintering, the relative density can be directly projected from the linear shrinkage and initial/final relative densities. As ZnO cold sintering employs acetic acid solution as a transient phase in an open system, allowing it to mostly evaporate during the heating ramp, the rapid linear shrinkage between 3 and 6 minutes may be recognized as the combined effects of powder densification and liquid evaporation. However, thermal gravimetric analysis (TGA) of the wet green body showed that the weight loss was only 3% of the total weight up to 120 °C (Fig. S4, ESI†), despite the initial 15 wt% of the added transient phase. Hence, the TGA result indicates that following points:

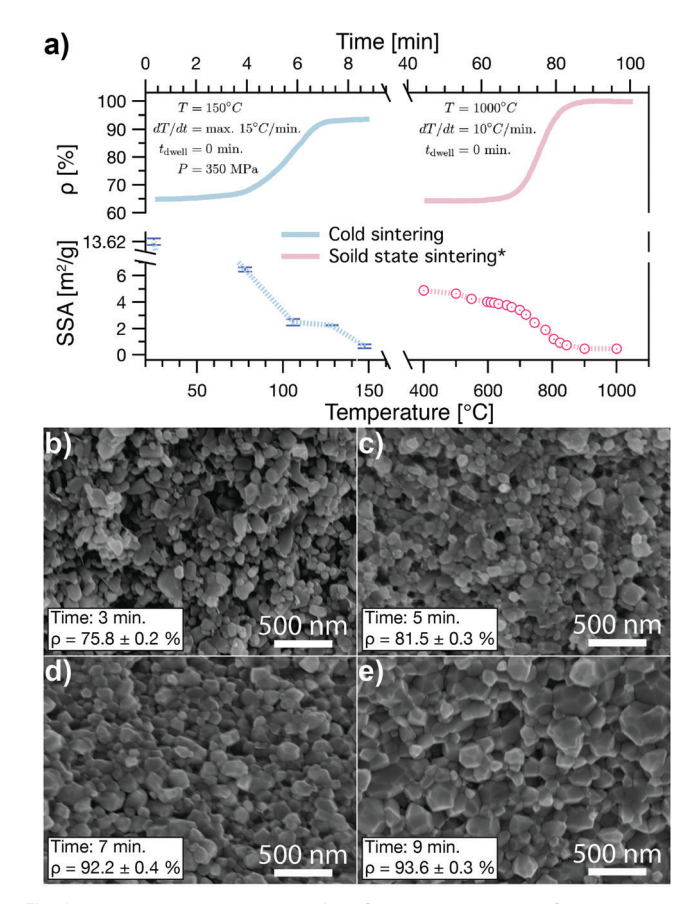


Fig. 1 Anisothermal sintering of ZnO powder under 350 MPa uniaxial pressure. (a) Comparisons to ZnO solid state sintering of the relative density $(\rho)^{33}$ and specific surface area (SSA)²⁸ as functions of temperature and time. (b-e) Microstructure evolution of the fracture surfaces at times of 3, 5, 7 and 9 minutes.

(1) excessive transient liquid can be extruded from the wet green body during the 5 minute pressure stabilization prior to cold sintering (Fig. S5, ESI†) and (2) liquid evaporation can be considered as only a minor effect for the linear shrinkage, as the remining liquid will be likely located in the pore spaces between particles.

Chemistry during the anisothermal sintering

The microstructural evolution verified that the fracture surfaces became significantly less porous and particles underwent more coarsening as the cold sintering progressed (Fig. 1b-e), where the 9 minute sample's microstructure, density and specific surface area sufficiently implied that the sintering process is already in the final stage. Regarding the phase purity through X-ray diffraction (Fig. S6, ESI†), zinc acetate complexes are a result of dissolution of zinc oxide powder and acetic acid solution. At elevated temperature, water begins to evaporate, the hydrate becomes anhydrous, and the following reactions may explain different pathways leading to the formation of phase pure ZnO:34-36

$$Zn(CH_3COO)_2(s) \xrightarrow{147-250\,^{\circ}C} ZnO(s) + (CH_3COO)_2O(g) \ \ (R1)$$

$$(CH_3COO)_2O + 4O_2 \rightarrow 4CO_2 + 3H_2O$$
 (R2)

$$Zn(CH_3COO)_2(s) + H_2O \xrightarrow{147-250\,^{\circ}C} ZnO + 2CH_3COOH \ \ (R3)$$

Here, (R1) describes the decomposition of zinc acetate into ZnO and acetic anhydride, which further reacts with oxygen to produce CO2 and H2O as shown in (R2). (R3) is reported for the case of a highly humid atmosphere where zinc acetate can react with water to form ZnO and acetic acid. Both reactions are reasonable for the given ZnO cold sintering, as its open system characteristic makes it accessible to oxygen and water. Considering the pressure solution creep mechanism as a governing mechanochemical process for cold sintering,³⁷ the dissolution of ZnO by acetic acid solution may produce zinc acetate complexes at the compressional grain boundaries, 38 which is consistent with XRD analysis. Once those complexes precipitate at low stressed pores, they undergo decomposition and produce ZnO, which mainly contributes to ZnO cold sintering being phase pure.

Quantifying the sintering activation energy

The linear shrinkage at different heating rates of cold sintering and solid state sintering30 was plotted (Fig. 2a). The corresponding temperature of the maximum linear shrinkage rate shifts towards a lower region for both sintering methods, which can be related to heating rate dependent kinetic processes.³⁹ Especially for cold sintering, as a slower heating rate can retain the transient phase longer, allowing a higher degree of solution-assisted particle rearrangement, more linear shrinkage was measured at temperatures below 65 °C. Regarding the anisothermal sintering activation energy estimation, the modified Woolfrey-Bannister method takes a data-driven approach based on eqn (4) to empirically determine n and its relevant uncertainty (Fig. S7, ESI†). It also needs to be noted that the shrinkage behavior can be

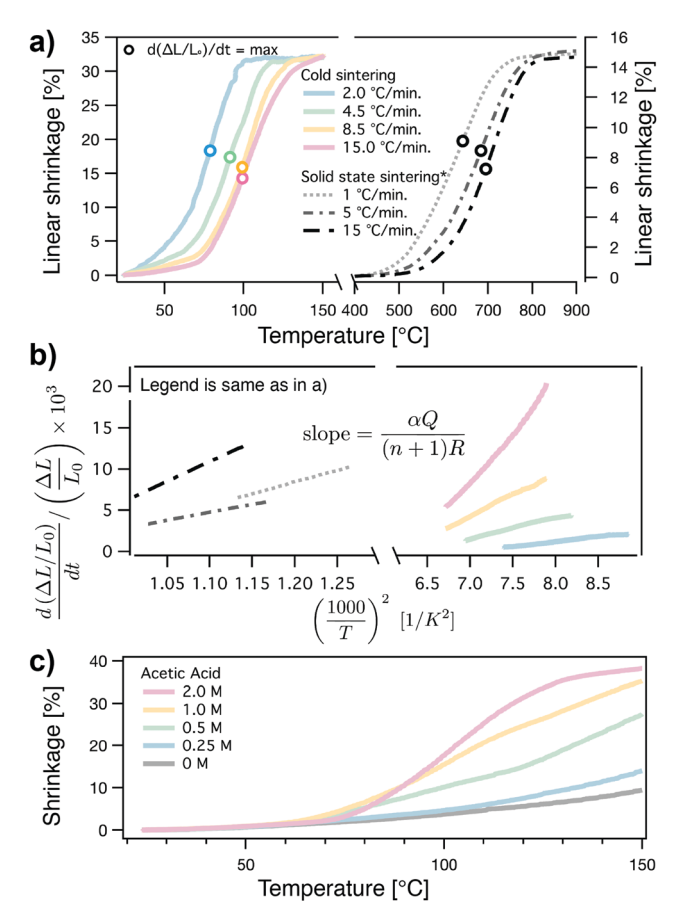


Fig. 2 (a) Linear shrinkage of ZnO cold sintering under 175 MPa and solid state sintering³⁰ at different heating rates, where the circle shows the maximum shrinkage rate. (b) Plot based on eqn (3), where the slope contains the activation energy term. (c) Linear shrinkage dependence on the concentration of acetic acid

roughly classified into three parts based on the shrinkage rate, and only the middle portion, featuring the maximum shrinkage rate, was considered in this proposed analysis. Analogous to the solid state sintering case, steep shrinkage is mainly related to the densification during cold sintering as the relative density evolves up to 93%. Therefore, the proposed method focuses on quantifying the activation energy of anisothermal sintering, where powder densification generally happens. According to eqn (3), the slope contains the heating rate (α) , experimental exponent (n)and activation energy (Q) (Fig. 2b), and final values are summarized in Table 1. For cold sintering, Q converges around 49 kJ mol⁻¹, where the highest heating rate has diverging and higher Q, which may be related to the reduced degree of the dissolution process, as the transient phase stays shorter in the system. In comparison, solid state sintering shows that the slowest heating rate completely diverges from the other two heating rates, which are within the uncertainty range. Perhaps such a low heating rate can provide sufficient thermal energy to drive grain coarsening through a surface diffusion mechanism in the low temperature region, also leading to a decrease in the surface area and thermodynamic driving force for sintering,³⁹ or the specific heating rate may contain a possible experimental

Table 1 ZnO anisothermal sintering activation energies at different heating rates, based on the modified Woolfrey-Bannister method

	Cold sintering		Solid state sintering	
$\frac{n}{Q \text{ [kJ mol}^{-1}]}$	9.09 ± 1.32 $2.0 ^{\circ}\text{C min}^{-1}$ $4.5 ^{\circ}\text{C min}^{-1}$ $8.5 ^{\circ}\text{C min}^{-1}$ $15.0 ^{\circ}\text{C min}^{-1}$	$47.1 \pm 6.1 \\ 51.4 \pm 6.7$.,	454 ± 128

artifact as the shrinkage slope evolution is slightly aberrant compared to the other two rates.

Shrinkage depending on the transient chemistry

Depending on the concentration of acetic acid, the linear shrinkage can be significantly changed (Fig. 2c), confirming that compatible transient chemistry is a key factor that enables any cold sintering process and mainly determines the anisothermal sintering kinetics.

Discussion

Classifying the stages of anisothermal sintering

Considering the slope change of the ZnO cold sintering shrinkage curves, at least three different dominant processes can be hypothesized, which include (1) solution-assisted particle rearrangement, (2) powder densification by pressure solution creep and (3) grain growth and pore removal (Fig. S8, ESI†). Such a claim can be considered as logical, as rearrangement will initially occur with the presence of uniaxial pressure and a liquid phase in the system, but eventually stops due to the loss of the liquid and the formation of coarse grains, making particle sliding less likely to continue.40

Phenomenological approach to investigate the kinetics

The proposed empirical method presents a fundamental framework to study anisothermal sintering kinetics, purely based on experimental data by controlling the heating rate. Unlike the predetermined exponent with a corresponding diffusion mechanism, a convincing physical interpretation of empirical n is not yet available. However, the concentration dependent shrinkage study indicated that *n* is indeed associated with the chemical activities of the transient phase. To the best of our knowledge, once more information on empirical n values of different materials and process conditions is accumulated, then it will be possible to find their implication as a characteristic value. Moreover, it needs to be pointed out that the original Woolfrey-Bannister method does not take external pressure into account, but using the empirical exponent may allow one to reflect the convoluted effects of applied pressure and the resulting chemical activity.

Possible deviation from Arrhenius behavior

One assumption of this work and many conventional sintering kinetic studies is the temperature dependence of the rate process. As many diffusional and chemical processes hold to Boltzmann statistical thermodynamics or Arrhenius controlled rates, 41 with a homologous temperature $(T/T_{\rm m})$ even lower than 0.142 and non-equilibrium chemical dynamics,43 there is a possible deviation from the Arrhenius limit, as also outlined by Eyring and others. 44-46 One of the most well known is the Vogel-Fulcher-Tammann equation describing the temperature dependence of glass viscous behavior.47 The importance of reminding ourselves of such departures is the fact that the relative magnitudes of the activation energies would change. Overall, more extensive data across more material systems is required to consider the nature of the physiochemical mechanisms for cold sintering.

Conclusion

An empirical approach for investigating anisothermal sintering kinetics was proposed to analyze the activation energies of two different sintering methods. This work verified that the activation energy of ZnO densification is inherently small for the cold sintering process with the aid of compatible transient chemistry. The proposed fundamental framework further contributed to improving the theoretical understanding of the cold sintering process and provided reliable kinetic data, which can be potentially used in developing a relevant analytical sintering model.

Conflicts of interest

There are no conflicts to declare.

Acknowledgements

We gratefully appreciate support from National Science Foundation (DMR-1728634) for enabling fundamental kinetic study. We also thank Penn State Materials Research Institute facilities and the support staff in the Materials Characterization Laboratory.

Notes and references

- 1 R. German, Sintering: from empirical observations to scientific principles, Butterworth-Heinemann, 2014.
- 2 J. Mackenzie and R. Shuttleworth, Proc. Phys. Soc., London, Sect. B, 1949, 62, 833.
- 3 M. Dürr, A. Schmid, M. Obermaier, S. Rosselli, A. Yasuda and G. Nelles, Nat. Mater., 2005, 4, 607.
- 4 Y. Yong, M. T. Nguyen, T. Yonezawa, T. Asano, M. Matsubara, H. Tsukamoto, Y.-C. Liao, T. Zhang, S. Isobe and Y. Nakagawa, J. Mater. Chem. C, 2017, 5, 1033-1041.
- 5 T. Hérisson de Beauvoir, A. Sangregorio, I. Cornu, C. Elissalde and M. Josse, J. Mater. Chem. C, 2018, 6, 2229-2233.
- 6 D. Grossin, S. Rollin-Martinet, C. Estournès, F. Rossignol, E. Champion, C. Combes, C. Rey, C. Geoffroy and C. Drouet, Acta Biomater., 2010, 6, 577-585.
- 7 G. Goglio, A. Ndayishimiye, A. Largeteau and C. Elissalde, Scr. Mater., 2019, 158, 146-152.

- 8 A. Ndayishimiye, M. Y. Sengul, S. H. Bang, K. Tsuji, K. Takashima, T. H. de Beauvoir, D. Denux, J. M. Thibaud, A. C. van Duin, C. Elissalde and G. Goglio, *J. Eur. Ceram. Soc.*, 2020, **40**(4), 1312–1324.
- 9 C. A. Randall, J. Guo, A. Baker, M. Lanagan and G. Hanzheng, *Cold sintering ceramics and composites*, *US Pat.* App. 15/277, 2017, vol. 553.
- 10 K. Tsuji, A. Ndayishimiye, S. Lowum, R. Floyd, K. Wang, M. Wetherington, J. P. Maria and C. A. Randall, *J. Eur. Ceram. Soc.*, 2020, 40(4), 1280–1284.
- 11 J. Guo, B. Legum, B. Anasori, K. Wang, P. Lelyukh, Y. Gogotsi and C. A. Randall, *Adv. Mater.*, 2018, 30, 1801846.
- 12 S. H. Bang, T. H. de Beauvoir and C. A. Randall, *J. Eur. Ceram. Soc.*, 2019, **39**, 1230–1236.
- 13 T. H. de Beauvoir, S. Dursun, L. Gao and C. Randall, *ACS Appl. Electron. Mater.*, 2019, **1**(7), 1198–1207.
- 14 T. Ibn-Mohammed, C. A. Randall, K. Mustapha, J. Guo, J. Walker, S. Berbano, S. Koh, D. Wang, D. Sinclair and I. Reaney, J. Eur. Ceram. Soc., 2019, 39, 5213–5235.
- S. H. Bang, K. Tsuji, A. Ndayishimiye, S. Dursun, J.-H. Seo,
 S. Otieno and C. A. Randall, *J. Am. Ceram. Soc.*, 2020, 103,
 2322–2327.
- 16 B. Dargatz, J. Gonzalez-Julian and O. Guillon, Sci. Technol. Adv. Mater., 2015, 16, 025008.
- 17 M. Y. Sengul, J. Guo, C. A. Randall and A. C. van Duin, *Angew. Chem.*, 2019, 131(36), 12550–12554.
- 18 S. Funahashi, J. Guo, H. Guo, K. Wang, A. L. Baker, K. Shiratsuyu and C. A. Randall, *J. Am. Ceram. Soc.*, 2017, 100, 546–553.
- 19 J. Gonzalez-Julian, K. Neuhaus, M. Bernemann, J. P. da Silva, A. Laptev, M. Bram and O. Guillon, *Acta Mater.*, 2018, 144, 116–128.
- 20 M.-Y. Chu, M. N. Rahaman, L. C. D. Jonghe and R. J. Brook, J. Am. Ceram. Soc., 1991, 74, 1217–1225.
- 21 H. Palmour, Science of sintering, Springer, 1989, pp. 337-356.
- 22 R. Floyd, S. Lowum and J.-P. Maria, Rev. Sci. Instrum., 2019, 90, 055104.
- 23 M. Gropyanov and G. Abbakumov, *Sci. Sintering*, 1975, 7, 3–15.

- 24 V. Ivensen and V. Belen'kii, *Powder Metall. Met. Ceram.*, 1990, 29, 611–615.
- 25 S. Salem and A. Salem, Thermochim. Acta, 2014, 575, 322-330.
- 26 M. Kovalchenko, Y. G. Tkachenko, D. Yurchenko and V. Britun, *Powder Metall. Met. Ceram.*, 2014, 53, 180–190.
- 27 J. Woolfrey and M. J. Bannister, J. Am. Ceram. Soc., 1972, 55, 390–394.
- 28 L. Perazolli, E. Longo and J. A. Varela, *Sintering technology*, Marcel Dekker, 1996, pp. 77–84.
- 29 J. Han, A. Senos and P. Mantas, J. Eur. Ceram. Soc., 1999, 19, 1003–1006.
- 30 N. Neves, R. Barros, E. Antunes, I. Ferreira, J. Calado, E. Fortunato and R. Martins, *J. Am. Ceram. Soc.*, 2012, **95**, 204–210.
- 31 T. K. Roy and A. Ghosh, Ceram. Int., 2014, 40, 10755-10766.
- 32 W. S. Young and I. B. Cutler, *J. Am. Ceram. Soc.*, 1970, 53, 659–663.
- 33 F. Zuo, A. Badev, S. Saunier, D. Goeuriot, R. Heuguet and S. Marinel, *J. Eur. Ceram. Soc.*, 2014, 34, 3103–3110.
- 34 A. Moezzi, A. McDonagh, A. Dowd and M. Cortie, *Inorg. Chem.*, 2012, **52**, 95–102.
- 35 Z. Xia, Y. Wang, Y. Fang, Y. Wan, W. Xia and J. Sha, *J. Mater. Chem. C*, 2011, **115**, 14576–14582.
- 36 T. Arii and A. Kishi, Thermochim. Acta, 2003, 400, 175-185.
- 37 F. Bouville and A. R. Studart, Nat. Commun., 2017, 8, 14655.
- 38 D. Elliott, Geol. Soc. Am. Bull., 1973, 84, 2645-2664.
- 39 R. Brook, Proc. Br. Ceram. Soc., 1982, 32, 7-24.
- 40 V. Skorokhod, Powder Metall. Met. Ceram., 1999, 38, 350-357.
- 41 S. Arrhenius, Z. Phys. Chem., 1889, 4, 226-248.
- 42 M. Ashby, Acta Metall., 1974, 22, 275-289.
- 43 M. Y. Sengul, C. A. Randall and A. C. van Duin, *ACS Appl. Mater. Interfaces*, 2018, **10**, 37717–37724.
- 44 H. Eyring, J. Chem. Phys., 1935, 3, 107-115.
- 45 V. Aquilanti, N. D. Coutinho and V. H. Carvalho-Silva, *Philos. Trans. R. Soc.*, *A*, 2017, 375, 20160201.
- 46 V. H. Carvalho-Silva, N. D. Coutinho and V. Aquilanti, *Front. Chem.*, 2019, 7, 380.
- 47 A. K. Varshneya and J. C. Mauro, *Fundamentals of Inorganic Glasses*, Elsevier, 2019.